

Controlling Magnetic Coupling between Cobalt Nanoparticles through Nanoscale Confinement in Hexagonal Mesoporous Silica

Adam F. Gross, Michael R. Diehl, Kristen C. Beverly, Erik K. Richman, and Sarah H. Tolbert*

Department of Chemistry and Biochemistry, University of California at Los Angeles, Los Angeles, California 90095-1569

Received: January 29, 2003

Cobalt nanoparticles are incorporated into hexagonal honeycomb mesoporous silica to study the effect of nanoscale confinement on magnetic coupling. The superparamagnetic Co particles can fill a significant fraction of the total pore volume and can constitute up to $22.1 \pm 0.9\%$ by mass of the composite. We find that Co particles form chains in the silica pores, which results in altered magnetic coupling. For example, coupling within chains of Co particles in pores produces a higher coercivity than the value found in either noninteracting or randomly aggregated particles. Remanence measurements also indicate that the Co nanoparticles form ferromagnetically coupled chains, thus converting the structural anisotropy of the silica host into magnetic anisotropy in the guest. This work demonstrates a method to create anisotropy in a nanoscale composite using easily synthesized isotropic building blocks.

Introduction

Finite size effects in metallic magnetic nanocrystals results in particles with unique properties that are strongly dependent on size, shape, crystallographic structure, and defect distribution.^{1,2} As the particle size decreases, the coercivity decreases until thermal fluctuations overcome pinning of the spins to energetically favorable easy axes. At this point, the originally ferromagnetic particle becomes superparamagnetic and the spins can rotate freely between the easy axes.³ The barrier for this transformation is dependent on particle structure. In order for small metallic nanoparticles to be useful for magnetic recording or other hard-magnetic applications, they need to be ferromagnetic at room temperature. One solution is to make very hard magnetic particles that transform to the superparamagnetic phase well above ambient temperature.^{4,5} Another complementary option is to build anisotropy, such as a rodlike structure, into the particles.⁶ This deepens the energetic potential of the easy axes so the particles remain ferromagnetic at elevated temperature.

Our solution to this problem is to build up an anisotropic material out of isotropic, easy to synthesize colloidal building blocks. We start with round magnetic nanoparticles, which are stacked in chains to create anisotropic coupling. Stacking nanomagnets results in magnetic dipole–dipole coupling between particles.^{1,7} Such stacked nanoparticles should thus behave more like single elongated particles, with magnetic reversal behavior that differs from an isolated nanocrystal.⁷ A harder magnet should be created, and the easy axis should now be along the particle chain axis. By controlling coupling we are thus able to enhance the magnetic properties of the particles while still using a simple, well-developed nanocrystal synthesis.

Small round magnetic nanoparticles can be made of Co,^{8–12} FePt,^{4,5} Fe₃O₄,¹³ Fe₂O₃,¹⁴ CoPt₃,¹⁵ BaFe₁₂O₁₉,¹⁶ and a range of mixed metal ferrites.^{17–19} We chose cobalt nanoparticles because of the well-developed syntheses that result in facile control of

particle diameter, size distribution, and crystal phase. In addition, Co particles have a large magnetic moment per Co atom.⁹ These nanocrystals may be synthesized in a hexagonal close-packed (hcp), face centered cubic (fcc), or a cubic β -Mn phase known as the epsilon (ϵ) phase that is not found in bulk Co.^{1,8,10,11,20} All three phases are found in round particles, and disks of hcp-Co can be formed as well.^{11,20} Neither fcc-Co nanoparticles nor hcp-Co nanoparticles are very round as synthesized; however, ϵ -Co particles are formed as single-domain, round nanoparticles that are stable in solution.^{10,20} These qualities are important because magnetic properties of Co nanoparticles are very dependent on size and shape. The ϵ -Co nanocrystals are ideal for the present study due to their homogeneous volume distribution and near perfect cubic crystal structure. These crystallographic properties result in more uniform magnetic properties, compared to less perfect fcc or hcp samples. We note, however, that slight shape imperfections do generally result in an overall uniaxial anisotropy, even for ϵ -Co nanocrystals.¹ The net anisotropy is small, on the order of the fcc bulk anisotropy,²¹ which is an order of magnitude smaller than that of hcp cobalt. With this low internal anisotropy, changes in magnetic properties of the Co chains will not be greatly influenced by local crystallographic orientation of the particles and can be controlled instead by the nanoscale arrangement of the nanocrystals.

To encourage chainlike coupling between particles, we incorporate nanocrystals into the 1-dimensional pores of large pore *p6mm* hexagonal mesoporous silica (SBA-15) through a liquid-phase incorporation with a solution containing Co nanoparticles.²² It has been shown that coupling uniaxial particles in 1-dimensional chains causes magnetizing effects, such as an increase in coercivity.^{23,24} As more particles are linearly coupled, the magnetizing effects increase.²³ However, random dipole–dipole coupling between particles, such as in agglomerated particles, results in demagnetizing interactions.^{24,25} Even in well dispersed particles at 4% concentrations, demagnetizing effects from random coupling are still observed.¹ Only a nearly perfect monolayer of nanoparticles, which is very difficult to make,

* To whom correspondence should be addressed. E-mail: tolbert@chem.ucla.edu.

results in magnetizing interactions.^{26,27} Nanoscale confinement in pores only slightly wider than a single particle diameter should encourage the formation of chains while limiting demagnetizing isotropic interparticle coupling.

Mesoporous silica is an ideal host material to use in host/guest chemistry. It is made by synthesizing a silica/surfactant composite and calcining the material to remove the organic phase.²⁸ The hexagonal pore diameter can be controlled between 10 and 200 Å by changing the organic template and by changing synthesis conditions.^{22,29} The calcined material has a narrow pore size distribution and a high surface area. The silica can easily be treated with chlorosilanes to attach a functional group that alters the surface chemistry and polarity of the silica.³⁹ Many phases of silica/surfactant composites can be synthesized,^{22,30–33} but we are most interested in the *p6mm* hexagonal phase (SBA-15) for nanoscale confinement of Co nanoparticles because it contains linear, 1-dimensional pores that are the correct diameter to force Co particles to stack in chains.

Many techniques have been developed to fill mesoporous materials with a variety of guest species. Mesoporous silica has been filled with Au, Pt, and PbS nanowires and nanoparticles.^{34–38} Moderately high filling fractions can be obtained by thermally degrading or reducing a precursor that is impregnated into the pores using liquid-phase incorporation.^{34–37} Alternatively, including nanoparticles in the synthesis mixture yields a material with few, well dispersed particles in the organic regions of the composite.³⁸ Studies of the effect of placing guest materials in the controlled geometries of a hexagonal porous host show that incorporation changes the properties of the guest material. For example, confinement of MEH–PPV, a semiconducting polymer, in the aligned pores of hexagonal mesoporous silica results in a material with strong fluorescence anisotropy.³⁹ It was also found that nanoscale confinement of PbS in pores results in a blue shift in the photoluminescence relative to bulk PbS. Finally, incorporating cobaltocene into the pores of mesoporous niobium oxide and reducing the material results in a superparamagnetic material, even though cobaltocene is always paramagnetic in the bulk.⁴⁰ It is not understood why the magnetic state of cobaltocene changes, and so a better understanding of the effect of placing a magnetic material in a controlled geometry motivates this work. To date, mesoporous materials have not been filled with externally synthesized magnetic metal nanoparticles. We believe that magnetic interactions between colloids may provide a driving force to realize even higher filling fractions of the silica host. In addition, higher quality magnetic materials with a chosen crystal phase and fewer defects can be produced with externally synthesized nanoparticles, which will simplify the analysis of magnetic data.

We note that an alternative method to fill a mesoporous template is to grow nanowires electrochemically in the pores of a polymer or alumina membrane that is in contact with an electrode.^{6,41–43} The pores in these templates are generally much larger than those in mesoporous silica, but they have the advantage that they can be made perpendicular to the substrate. The types of materials that can be produced electrochemically are limited, however, and control of the crystal phase of the wires grown electrochemically is not always possible. A significant advantage to electrochemical filling is that it produces high-filling fractions and easily controllable nanowire shape anisotropy.

In this work, we use a variety of techniques to understand how nanoscale confinement affects magnetic coupling in Co/SiO₂ composite assemblies. X-ray diffraction is used to inspect the phase of the Co nanocrystals and the periodicity of the

nanoporous silica. N₂ absorption/desorption provides information on the silica pore size, and TEM is used to image the Co/SiO₂ composite. ICP/AE is run on digested Co/SiO₂ composite to find the filling fraction of Co in the material. Finally, SQUID magnetometry is used for investigating coupling between Co nanocrystals.

Experimental Section

SBA-15 was synthesized using the method presented in ref 22. Briefly, 4 g of P123 were dissolved in 30 g of water and 120 g of 2 M HCl. Next, 8.5 g of tetraethyl orthosilicate (TEOS) was added and the solution was stirred for 6 h at room temperature. The mixture was heated to 60 °C with stirring for 3 days, followed by 1 day of hydrothermal treatment at 100 °C, after which the SBA-15 was recovered by filtering. The SBA-15 was calcined in air by heating to 500 °C at 1 °C/min, holding at 500 °C for 6 h, and then cooling to room temperature over 3 h.

To make the silica surface nonpolar, the mesoporous silica was silylated with chlorotrimethylsilane.³⁹ The calcined SBA-15 is first dried at 450 K under vacuum for 4 h to remove any water. Under standard air free conditions, a few drops of triethylamine were first added to the silica, followed by neat trimethylchlorosilane. The reaction mixture was stirred for 1 h at room temperature, then filtered, washed with hexane, and heated at 100 °C for 1 h under N₂. N₂ absorption/desorption data were collected to determine pore size and surface area using a Micromeritics ASAP 2000 porosimeter. The density of the silylated silica framework was determined using a Micromeritics Accupyc 1330.

Co particles are synthesized by thermal decomposition of Co₂(CO)₈.^{10,11} In the synthesis, 0.2 g of trioctylphosphine oxide (Alfa Aesar) and 0.1 mL of oleic acid (99%, Aldrich) were mixed with 15 mL of dry *o*-dichlorobenzene (ODCB, Aldrich) and heated to 180 °C under vigorous stirring. Next, 0.36 g of Co₂(CO)₈ mixed with 3 mL of ODCB was injected, followed 30 s later by removal of the heat source to quench the reaction. When the synthesis solution cooled below 40 °C, a few drops of oleic acid were added to passivate the particles. All steps were performed under Ar. Although our reaction time and reagent quantities differ from the values that made the best ϵ -Co particles in refs 10 and 11, we found they made the best nanoparticles in our laboratory.

To prepare samples for magnetometry, the cobalt synthesis solution was first centrifuged to remove pieces of Co metal and agglomerated particles. The supernatant was then used in all of the following sample preparations: Dilute and concentrated Co particles were made by first precipitating the synthesis solution with dry ethanol and centrifuging the solution. Concentrated particles were obtained by collecting the solid, whereas dilute particles were made by redissolving the precipitate in dodecane and a few drops of oleic acid. Both samples were then placed under vacuum to remove any excess ethanol. Particles were impregnated into pores by mixing 3 mL of the original synthesis supernatant with 0.20 g of silylated SBA-15 that had been under vacuum for at least 4 h to remove absorbed molecules. After 24 h, the silica and Co mixture was filtered in a glovebox. The Co/SiO₂ composite was washed with hexane while a few drops of oleic acid were added to remove any particles from the silica surface. The sample was washed quickly with dry methanol to passivate the particle surfaces and again with hexane. Samples with less Co in the pores were made by first diluting the synthesis solution with ODCB.

Wide-angle X-ray diffraction patterns were collected using Mo K α radiation from a Rigaku UltraX 18 rotating anode X-ray

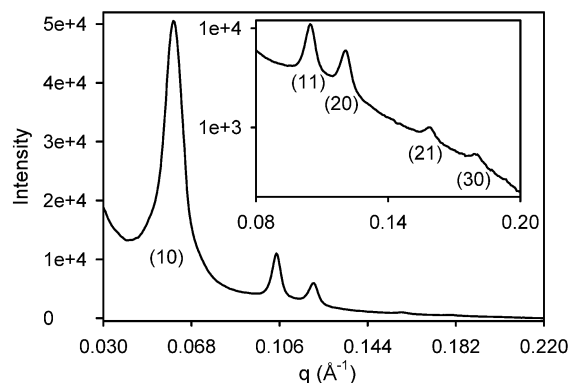


Figure 1. Low-angle X-ray diffraction pattern from calcined and chlorotrimethylsilane treated mesoporous silica synthesized using the triblock copolymer P123 as a templating agent. All peaks are indexed in parentheses to a $p6mm$ hexagonal honeycomb structure; the inset is an enlargement of the higher order peak region. This material has 86 Å diameter pores and a surface area of 450 m²/g.

generator and observed with a Roper Scientific X-ray CCD camera. Low-angle XRD was collected at the Stanford Synchrotron Radiation Laboratory on beamline 1–4 using 0.1488 nm X-rays.

SQUID magnetometry was collected using a Quantum Design MPMS with dc detection. TEM imaging was performed on a Phillips EM420 with an accelerating voltage of 120 keV and on a Hitachi H6000 with an accelerating voltage of 100 keV. ICP/AE analysis for cobalt was performed using a Thermo Jarrell Ash Corp. Iris 100. A 1000 ppm Co standard (Aldrich) was used to make calibration standards. Samples were prepared by soaking and sonicating the Co/SiO₂ composite in aqua regia to dissolve the cobalt colloids. The amount of solvent in the composite was found by heating materials in a Perkin-Elmer TGA 2950 thermogravimetric analyzer under nitrogen at a rate of 10 °C/min.

Results and Discussion

A. Materials Characterization. To control interactions between cobalt particles, a well-ordered matrix is needed. Figure 1 shows low-angle XRD of the silylated mesoporous silica. Five peaks indexing to a $p6mm$ 2-dimensional hexagonal structure are observed, which indicates very good nanoscale order. N₂ absorption/desorption measurements show that this material has 86 Å pores and a surface area of 450 m²/g.

High-quality ϵ -Co nanoparticles were synthesized using an established synthesis.^{10,11} Figure 2, bottom trace, shows XRD of the nanoparticles before incorporation. All peaks index to a β -Mn structure, proving that the particles are indeed ϵ -Co.⁸ Fitting the data to the Scherrer equation results in a nanocrystal diameter of 60 Å.⁴⁴ After liquid-phase incorporation of the Co particles and extensive washing with hexane to remove unincorporated colloids from the Co/SiO₂ composite, the high-angle XRD of the composite looks identical to that of pure particles (Figure 2, top trace). Because no increase in XRD peak widths occurs, impregnation of Co into the mesoporous silica appears to not damage the nanocrystals.

Figure 3 shows TEM images of the Co/SiO₂ composite. The top image shows that, in general, the Co is densely packed in the silica matrix and the nanocrystals are arranged in rows. No lattice fringes from the hexagonal silica are visible because the electron density of Co is much higher than that of SiO₂. Figure 3, middle, however, captures both low- and high-density regions of the composite. In this image, both rows of Co nanocrystals and the underlying periodicity of the nanoporous silica host can

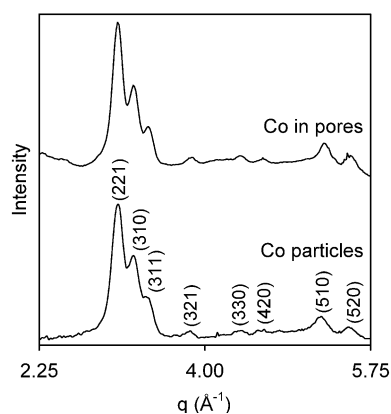


Figure 2. X-ray diffraction from ϵ -Co nanoparticles before incorporation into mesoporous silica (bottom) and in the Co/SiO₂ composite (top). All peaks, both before and after incorporation, index to a β -Mn structure, thus confirming that all of the nanocrystals are in the ϵ -Co phase. Because the peak widths do not broaden, the particles do not appear to be damaged by impregnation into the mesoporous silica.

be observed. In Figure 3, bottom, rows of Co particles in the silica host, indicated by white arrows, can be seen in a much higher resolution TEM image. The mesoporous silica has large regions that are concentrated with Co, like the image shown Figure 3, top, but also some empty regions. Such concentration and spatial variations may be indicative of cooperative effects where dipole–dipole coupling between particles helps produce very high-filling fractions in some regions.

B. Magnetic Properties of Co Nanocrystals in Different Environments. Our goal is to understand how the geometry of the hexagonal pore controls dipole–dipole coupling between particles. Magnetometry is useful because it provides information on the nature of interparticle coupling. To understand the magnetometry data from particles in pores, we compare it to data from both a noninteracting system such as dilute Co particles and a randomly interacting system such as concentrated particles. One particularly informative type of magnetometry data is magnetic hysteresis curves.² The hysteresis width, or coercivity, is related to the energy to reverse the direction of magnetization in a ferromagnet. The hysteresis width for noninteracting single-domain nanoparticles only depends on the internal crystal structure of a particle.⁴⁵ This case is analogous to our dilute Co particles. Isotropic interactions between particles, such as in agglomerated or concentrated particles, cause a reduction in coercivity by decreasing the barrier for magnetization reversal.⁴⁶ It has been shown, however, that ferromagnetically coupling uniaxial particles in chains should result in an increase in coercivity.²³ This is due to a constructive addition of the potentials for magnetization reversal. As the chain length increases, so should the hysteresis width.²³

If a sample is held at low temperature, the width of a hysteresis curve can be used to learn about the barrier for magnetization reversal. Low temperature is important because the contribution of thermal energy is removed and the measured hysteresis width indicates the actual barrier height. Figure 4 shows hysteresis curves collected at 5 K for all three samples. A dilute ϵ -Co sample has a hysteresis width of 1550 Oe, a sample of concentrated nanoparticles has a coercivity of 450 Oe, and a hexagonal Co/SiO₂ composite has a coercivity of 2450 Oe. The hysteresis width of 1550 Oe is the coercivity of our particles in the absence of interactions. Values larger than this signify the presence of magnetizing interactions, whereas a smaller coercivity is evidence of demagnetizing interactions. The small hysteresis width in concentrated particle data indicates

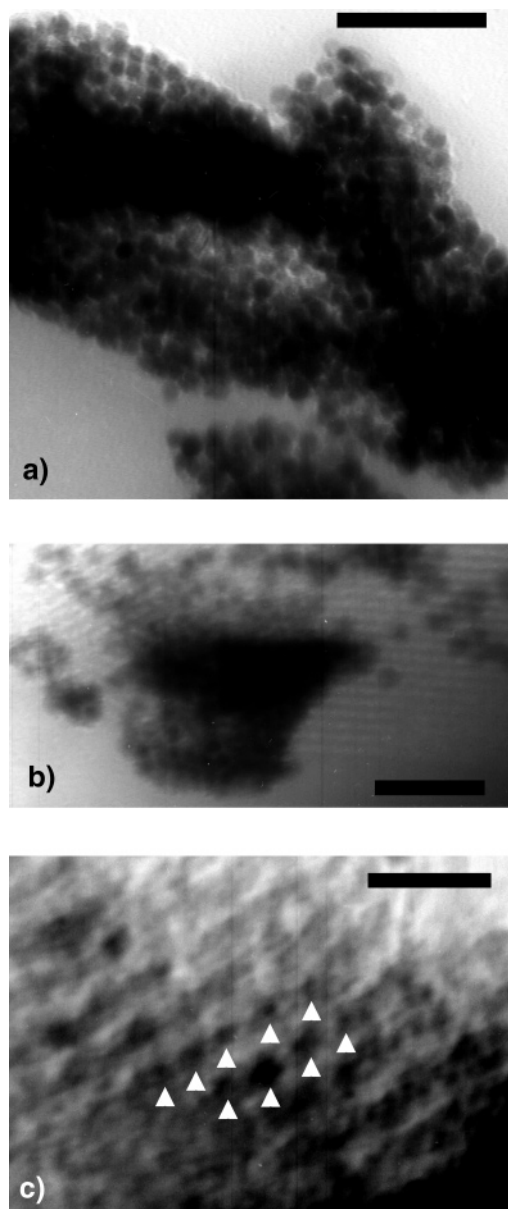


Figure 3. (a) TEM image of a mesoporous silica densely filled with Co particles. The Co nanocrystals are observed to arrange roughly in lines, but because of the high electron density of Co, it is difficult to see the silica framework in this highly filled composite. The black scale bar corresponds to 100 nm. (b) Both densely filled and sparsely filled regions of mesoporous silica are visible in this image of a Co/silica composite. In the sparse regions, the nanoscale periodicity of the silica host can be clearly observed. The scale bar again corresponds to 100 nm. (c) In this high-resolution TEM image, chains of evenly spaced Co nanocrystals are visible within the silica channels. Particles are marked with white arrows and the scale bar corresponds to 20 nm.

that random, isotropic interactions are present in this sample. However, we observe the largest coercivity in the Co/SiO₂ composite. The fact that the coercivity of the Co/SiO₂ composite is greater than dilute particles indicates that coupling in chains dominates over isotropic interaction in this sample. This idea is in good agreement with TEM observations that show particles lined up in chains (Figure 3).

We learn more about domain structure and interparticle coupling in our samples by the observation of zero field cooled/field cooled (ZFC/FC) magnetization curves. For the ZFC experiments, a sample is cooled with no field on and then heated in a small field while the net magnetization of the sample is recorded. The FC data are produced by cooling particles in a

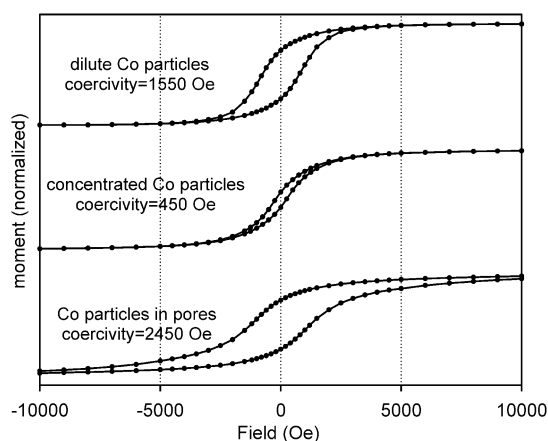


Figure 4. Hysteresis curves taken at 5 K for dilute Co nanoparticles, concentrated Co nanoparticles, and Co nanoparticles incorporated into a hexagonal mesoporous silica. All curves are labeled on the graph. The hysteresis width, or coercivity, shows how well a material retains its direction of magnetization. There are no interactions between dilute particles, so the coercivity of 1550 Oe is only determined by the particle crystal structure and its shape and surface anisotropy. In concentrated Co particles, random dipole–dipole coupling occurs and greatly reduces the coercivity to 450 Oe. Anisotropic coupling in the 1-dimensional pores of the mesoporous silica causes constructive coupling between particles, which results in the largest hysteresis width observed (2450 Oe).

small field after the ZFC experiment and recording the change in net sample magnetization with temperature. At the start of a ZFC experiment (Figure 5, top), the magnetic moment of each atom is randomly frozen to an easy axis of a particle. Because the particles are not aligned in any direction, the net magnetization is small once a field is applied. As the temperature increases, the data show an increase in net magnetization as thermal energy frees the spins from their alignment along the particle easy axis and allows them to align with the applied field.⁸ A ferromagnet exhibits a monotonic increase in the ZFC data with increasing temperature. In superparamagnetic systems, however, the net magnetization increases and then decreases with increasing temperature because thermal fluctuations cause a decrease in the net degree of alignment at high temperatures. The peak in the magnetization is known as the blocking temperature and it is the transition point between ferromagnetic and superparamagnetic behavior. This transition occurs when the thermal energy becomes greater than the barrier height for magnetization reversal. In superparamagnetic systems, the blocking temperature can be used to study coupling between particles. An increase in interparticle magnetic coupling is known to shift the blocking temperature to higher temperature because the coupling suppresses thermal fluctuations of magnetic spins.⁸

The FC data also provide information about coupling between particles. In many types of magnetic systems, the net magnetization increases with decreasing temperature during a FC experiment. This is because thermal fluctuations decrease with decreasing temperature, and so the spins are better able to align with the applied field. Coupling between colloids naturally suppresses these fluctuations and thus the increase in net magnetization during a FC experiment relates inversely to the amount of interparticle coupling. Uncoupled systems show a large increase in FC data. Strongly coupled systems, however, show a much smaller rise in FC data because particle–particle interactions stabilize spins in their original configuration and prevent alignment with the field.

The domain structure and the relative amount of coupling in our dilute, concentrated, and nanoporous samples can be

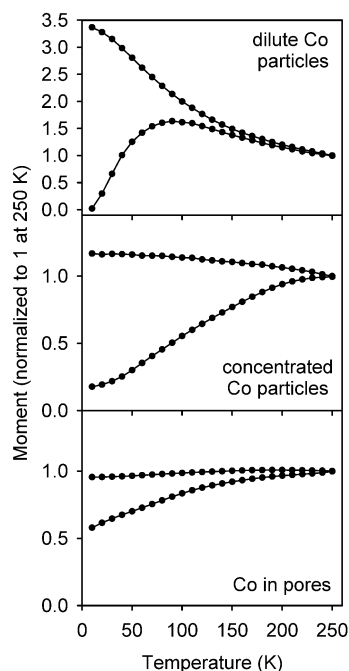


Figure 5. Zero field cooled/field cooled (ZFC/FC) magnetization curves for dilute Co nanocrystals (top), concentrated Co nanocrystals (middle), and Co nanocrystals incorporated into mesoporous silica (bottom). The low blocking temperature of 90 K and the large rise in the FC magnetization data with decreasing temperature in the top panel for dilute particles are both indicative of noninteracting superparamagnetic nanoparticles. In the concentrated particles (middle), the observation of a blocking temperature above 250 K in the ZFC magnetization data and very small rise in the FC magnetization data with decreasing temperature signify strong interactions between nanocrystals. In the bottom panel, the shallow rise in the ZFC magnetization curve with increasing temperature and the almost flat FC curve indicate that strong dipole–dipole coupling is also present in the hexagonal Co/SiO₂ composite.

deduced from ZFC/FC magnetization curves in a 25 Oe field shown in Figure 5. All data are normalized to 1 at 250 K. The dilute particle sample has a 90 K blocking temperature and a large increase in the FC magnetization with decreasing temperature; both are indicative of noninteracting particles. The blocking temperature above 250 K in the ZFC data and the small increase in the FC magnetization upon cooling from concentrated Co nanocrystals, by contrast, reveal significant interparticle coupling. The high blocking temperature in the ZFC curve for the Co/SiO₂ composite and flatness of the FC curve also indicate strong interparticle coupling. This result confirms our hypothesis that the broad hysteresis width in the Co/SiO₂ sample shown in Figure 4 is caused by uniaxial, space-controlled coupling in these materials, rather than resulting from a dilute sample that somehow lacks interparticle coupling.

C. Magnetic Properties of Co Nanocrystals with Different Filling Fractions. To understand the nature of coupling between particles in confined spaces, we need to first understand the structure of Co particle arrays in the silica matrix. Up to this point, we have been looking at magnetic colloids in fundamentally different arrangements. To gain more insight about the effect of colloid arrangement on magnetic properties, we perform a controlled experiment in which we fill samples of an identical silica host with different amounts of Co using the same batch of Co nanocrystals. There is some variation between samples, and by using the same batches of Co and mesoporous silica, the effect of differences between identically prepared samples should be eliminated. By filling mesoporous silica with different

amounts of Co, it may be possible to study materials with similar geometries but different chain lengths to better understand interparticle coupling in pores.

Dilution of the synthesis solution prior to impregnation into silica controls the amount of Co that enters the pores. Undiluted synthesis solution results in a Co/SiO₂ composite that is $22.1 \pm 0.9\%$ by mass Co, a 4:1 dilution of the synthesis solution results in a Co/SiO₂ composite that is $14.1 \pm 0.7\%$ by mass Co, and a 61:1 dilution of the synthesis solution results in a Co/SiO₂ composite that is $0.3 \pm 0.1\%$ by mass Co. The 14% Co composite has 47 times the concentration of Co in the 0.3% Co composite, but the impregnation solution was only 15 times as concentrated. Because the amount of Co in the composite increased 3 times faster than the change in concentration of the impregnation solution, this again suggests a cooperative filling mechanism. Magnetic particles have dipole–dipole interactions that result in attractions between particles. Once some Co particles are in a pore, they may induce others to enter. Saturation of this mechanism could also explain the difference in Co content of the 14% Co and 22% Co/SiO₂ composites. The 22% Co composite has 1.6 times the concentration of Co in the 14% Co composite, but the impregnation solution is 4 times as concentrated. In this case, a large amount of Co has already been brought into the mesoporous channels, but limited diffusion length inside the nanoscale pores may eventually cause pore access to be blocked.

The most meaningful metric to understand the incorporation of a guest species into a host is the fraction of the available space in the host that has been occupied. To better describe our materials, we thus convert our percent mass measurements to occupied volumes. All samples were $\sim 2\%$ by mass solvent (hexane, ODCB, and methanol) and $\sim 98\%$ Co, SiO₂, and capping ligands. The mass fraction of Co is known. The quantity of ligand (oleic acid and TOPO) was found by using the carbon content of ϵ -cobalt particles from ref 9 and scaling this to take into account the larger surface area-to-volume ratio of our smaller particles. The remaining mass that is not cobalt, solvent, or capping ligand must be silylated silica. Density measurements on the silylated SBA-15 indicate a wall density of 2.02 for the material. Using the fact that the silylated silica has 34 Å walls and 86 Å diameter pores, we calculate that 53.4% of the mesopore is empty; thus the overall density is 0.94 g/cm³. This information along with the density of ϵ -Co, 8.635 g/cm³, allows for calculation of volume fractions of Co in SBA-15. The volume occupied by a particle is calculated as the volume of a pore that is excluded from another Co particle by the incorporated nanocrystals and their organic capping ligands. For the $22.1 \pm 0.9\%$ by mass Co/SiO₂ composite, $31 \pm 2\%$ of the free space is filled by Co particles, for the $14.1 \pm 0.7\%$ by mass Co/SiO₂ composite, $18 \pm 2\%$ of the free space is filled by Co particles, and for the $0.3 \pm 0.1\%$ by mass Co/SiO₂ composite, less than 1% of the free space is filled by Co particles. The volume fractions we find, however, are averages and do not take into account local changes in Co particle density. In reality, for highly filled samples such as the 22% by mass Co/SiO₂ composite, we observe many Co particles adjacent to one another at near 100% volume fractions in some regions with TEM (Figure 3, top), whereas in other regions of the composite, the mesoporous silica is nearly empty.

We again learn about interparticle coupling and domain structure for the three Co/SiO₂ composites from hysteresis curves at 5 K (Figure 6) and ZFC/FC data (Figure 7). The 0.3% Co sample has a coercivity of 1100 Oe (Figure 6) and a blocking temperature of 170 K (Figure 7). The ZFC/FC curve showing

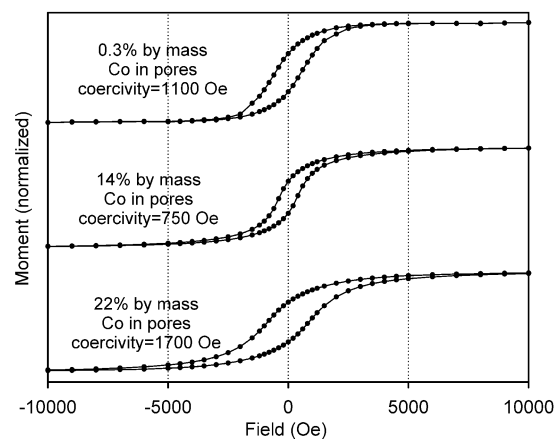


Figure 6. Hysteresis curves taken at 5 K for Co/SiO₂ composites containing different amounts of cobalt. All curves are labeled with the mass percent Co on the graph. The hysteresis width, or coercivity, shows how well a material retains its magnetization under a reversal field. The coercivity of the 0.3% by mass Co/SiO₂ composite resembles dilute particles, which suggests that few interactions are present in this material. In the 14% by mass Co/SiO₂ composite, random interactions dominate and a smaller hysteresis width is measured. In the 22% by mass Co/SiO₂ composite, however, chains of Co particles result in increased coercivity.

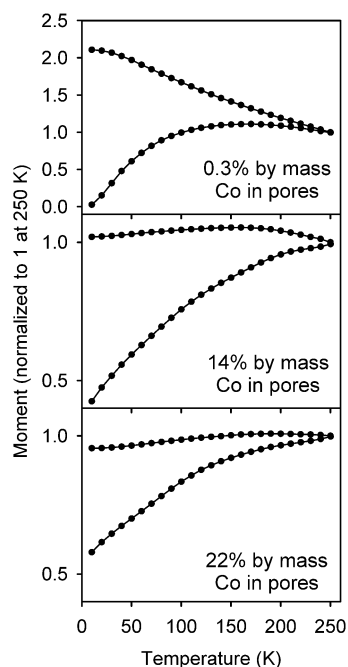


Figure 7. Zero field cooled/field cooled (ZFC/FC) magnetization curves for Co nanocrystal/hexagonal mesoporous silica composites containing 0.3% by mass Co (top), 14% by mass Co (middle), and 22% by mass Co (bottom). The blocking temperature of 170 K and the rise in the FC data with decreasing temperature in the 0.3% Co composite indicate only slightly interacting superparamagnetic nanocrystals (top). By contrast, the high blocking temperature (>250 K) in the ZFC data and the small peak in the FC data in the 14% Co composite signify strong interactions between nanocrystals with some anisotropic and some isotropic coupling in the pores (middle). Stronger anisotropic interactions are found in the 22% Co composite, which shows a steady drop in the FC magnetization data with decreasing temperature (bottom).

superparamagnetic behavior and the large rise in the FC data indicates low-concentration superparamagnetic Co nanoparticles. The smaller coercivity and higher blocking temperature relative to dilute particles, however, shows that there are some interactions between particles despite the high dilution. The 22% Co

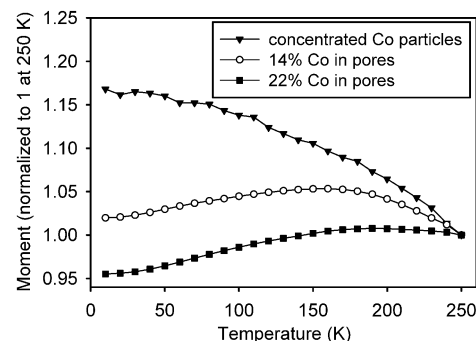


Figure 8. Field cooled (FC) magnetization data collected on concentrated Co nanoparticles and two Co in hexagonal nanoporous silica composites. The legend is on the graph. In the concentrated Co particles, isotropic coupling between nanoparticles limits alignment with the external applied field and results in a small rise in the FC magnetization with decreasing temperature. By contrast, in the 22% Co by mass composite, the FC magnetization drops as the temperature is lowered. This result occurs because of increased anisotropic coupling between nanocrystals in the pores of the mesoporous silica with decreasing temperature. Such coupling orients the magnetic moments along the pore axes and thus pulls the nanocrystal spins away from the direction of the external applied field. Data from the 14% Co by mass composite show contributions from both isotropically interacting concentrated particles (at higher temperature) and anisotropically coupled nanocrystals (at lower temperature). This sample probably contains short chains of nanocrystals.

by mass samples have a hysteresis width of 1700 Oe, which is smaller than the hysteresis width in Figure 4 for a Co/SiO₂ composite, but still larger than the coercivity of dilute particles. The data from the 14% by mass Co/SiO₂ composite have a much smaller hysteresis width (750 Oe) than found in dilute particles or the 0.3% or 22% Co by mass Co/SiO₂ composite. This suggests that there are random demagnetizing interactions between particles in this composite sample, as in concentrated Co particles. The ZFC magnetization data for the 14% and 22% by mass Co/SiO₂ composite also have blocking temperatures above 250 K, which again indicate strong interactions.

The data in Figures 7 and 8 help us to better understand how Co fills the pores of the hexagonal nanoporous silica. Co particles first enter the pores of mesoporous silica to form a fairly well dispersed composite (0.3% Co sample). The FC/ZFC data indicate that few chains are formed in the system. A more concentrated impregnation solution results in more particles entering the silica matrix due to a cooperative filling mechanism. Chains are formed, as shown by the flat FC magnetization data for the 14% by mass Co composite, but they are not long. Overall, demagnetizing interparticle interactions dominate in the 14% by mass composite, as shown by the small hysteresis width. As even more Co is impregnated, however, longer chains of Co nanocrystals are formed and a desirable increase in coercivity occurs in the 22% by mass Co/SiO₂ composite.

Differences in chain lengths can be qualitatively measured by comparing FC data for various highly coupled systems. As discussed previously, disordered concentrated nanocrystal samples show only a small increase in FC magnetization with decreasing temperature (Figures 5 and 8). By contrast, both the 14% and 22% Co composites show a *decrease* in the FC data (Figure 8), which demonstrates that coupling between particles is stronger than coupling to the applied field. Because the silica matrix is a powder, there is no net alignment of pores in each grain with the applied field. Thus there should be a random angular distribution of chains in the Co/SiO₂ composite. Strong coupling along the chains in the pores should increase the shape

anisotropy of the Co nanocrystals along the pore direction. Because only the projection of the magnetic moment along the applied field will contribute to the net magnetization of the sample, increased coupling within a chain will tend to orient spins along the pore axis and away from the direction of the applied field, thus decreasing the net magnetization. Alternatively, particles coupled antiferromagnetically have zero net moment, and so such coupling would also cause a net decrease in magnetization. Either type of intrachain coupling could thus explain the decrease in magnetization with decreasing temperature during a FC experiment. The 22% Co by mass Co/SiO₂ composite probably has the longest chains of any sample, which would result in the strongest intrachain coupling. Consequently, a monotonic decrease in the FC data is observed in the 22% Co sample. The FC data from the 14% Co by mass Co/SiO₂ composite look like a combination of data from concentrated and the 22% by mass Co/SiO₂ composite (Figure 8). The small hysteresis width observed in the 14% Co by mass Co/SiO₂ composite demonstrates that it contains only small chains and dispersed particles. It is thus reasonable that the FC magnetization data first increase slightly between 250 and 160 K as thermal disorder is removed and the colloids align with the applied field. The FC magnetization then decreases below 160 K as particles in small chains begin to couple with each other.

D. Magnetic Remanence. One final experiment can be used to confirm our hypothesis about the nature of interparticle coupling in our composites and to distinguish between ferromagnetic and antiferromagnetic coupling between nanoparticles within the pores. The magnetic remanence is the net magnetization at 0 applied field after application of a saturation field, divided by the saturation magnetization. This value yields information on the type of coupling between magnets in a sample. Dilute nonaligned, noninteracting, uniaxial ferromagnetic particles are predicted to have a magnetic remanence of 0.5, based simply on geometric considerations.⁴⁵ Particles with their easy axis aligned with the field will have a remanence of 1, whereas those aligned with the easy axis perpendicular to the applied field will have a remanence of 0. An average over all orientations results in a remanence of 0.5. By contrast, antiferromagnetically coupled dipoles have a remanence of 0. The magnetic remanence of our samples will thus allow us to discern the type of coupling in chains of Co in pores. Randomly oriented chains of ferromagnetically coupled ferromagnetic particles will also have a magnetic remanence of 0.5, on the basis of the same geometric arguments used for dilute particles.^{7,23} However, chains of antiferromagnetically coupled particles will have a remanence of 0, as spins will pair and their moments will cancel.

By following changes in remanence with nanocrystal geometry, we can deduce the type of coupling in the Co/SiO₂ composite. All remanence data are shown in Figure 9. Dilute Co nanoparticles have a remanence of 0.48, which agrees well with the theoretical remanence of 0.5 for randomly oriented noninteracting particles.⁴⁵ Concentrated Co particles have a remanence of 0.15, which results from demagnetizing interactions between particles. For a random distribution of easy axes, the magnetic moments of particles tend to cancel beyond the simple geometric factor, and a decrease in remanence is observed. The most dilute Co in silica sample (0.3% Co by mass) has a remanence of 0.38. This value is less than 0.5 because there are some demagnetizing interactions in this material. In agreement with the slightly elevated blocking temperature and the narrower hysteresis width in this sample, compared to dilute particles, there are some demagnetizing

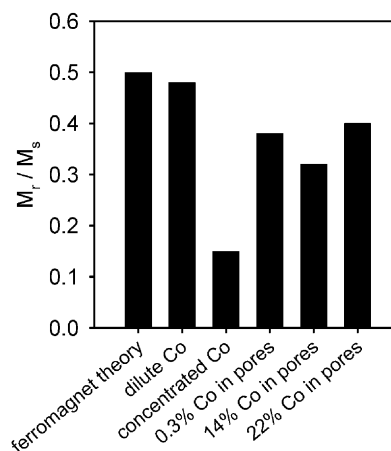


Figure 9. Magnetic remanence from Co nanocrystals can be used to understand the nature of interparticle coupling in chains. Isolated ferromagnetic particles or particles coupled ferromagnetically in chains should have a remanence of 0.5; demagnetizing interactions lower this value. Dilute Co particles have a remanence of 0.48, which is near the theoretical value. Demagnetizing isotropic interactions result in the reduced remanence of 0.15 for concentrated particles. As the mass fraction of cobalt in pores increases from 0.3% to 14%, the remanence decreases due to additional demagnetizing interactions. Chains appear to form in the 22% Co by mass Co/SiO₂ composite, as indicated by an increase in the remanence to 0.40. This increase confirms that particles are coupling ferromagnetically in chains in mesoporous silica composites.

interactions in this sample (Figures 4 and 5). When more Co is placed in the composite, the remanence drops to 0.32 in the 14% Co by mass Co/SiO₂ composite. The remanence decrease is predictable because the low coercivity in this sample suggests significant demagnetizing interactions. As even more Co is placed in the pores, however, the remanence significantly increases to 0.40 for the 22% Co by mass Co/SiO₂ composite, and even higher remanence values are observed for some highly filled samples. This increase in remanence correlates with a large increase in coercivity (Figure 3), which signifies chain formation. Because the remanence moves toward the value for ferromagnetically rather than antiferromagnetically coupled particles when chains are formed, we conclude that particles in chains are coupled ferromagnetically in the pores.

The conclusion of ferromagnetic coupling in our samples is reasonable when we compare our particle arrangements to those of larger antiferromagnetically coupled chains in the literature.⁴⁷ Antiferromagnetic coupling between particles has only been observed when elliptically shaped nanomagnets are arranged lithographically with their long axes perpendicular to the chain axis. Neither round particles nor elliptical particles with their long axis along the chain tend to couple antiferromagnetically. Our Co/SiO₂ composites are made of either randomly oriented uniaxial particles in pores or slightly elliptical particles with the long axis along the pore. Because the pores are only slightly larger than the Co particles, it would be difficult for an elliptical particle to have its long axis perpendicular to the pore direction. Ferromagnetic coupling in chains is thus both the expected and desired result.

Conclusions

Nanoscale confinement of single-domain magnetic nanoparticles in the one-dimensional pores of hexagonal mesoporous silica results in constructive magnetic interactions. A more coercive material is formed due to anisotropic ferromagnetic interparticle coupling within the chains of nanocrystals. Control-

ling coupling between particles allows shape anisotropy to be created from easy to synthesize isotropic nanomagnets. Because it is not currently possible to make Co nanorods, this is a good alternative method to realize control over both the magnitude of barrier heights and the direction of magnetization through shape anisotropy.

It would then be interesting to anneal the composite to explore quantum mechanical coupling, where the nature of the coupling would be directed in part by the template. Moreover, this technique for making a magnetic composite can be generalized to any magnetic nanoparticle system. For example, the introduction of magnetic particles that are ferromagnetic at room temperature into a mesoporous matrix could result in an even harder magnetic material.⁴ In addition, by filling a conductive mesoporous framework with magnetic nanoparticles, magnetic–electronic coupling between the host and the guest might be realized.

Acknowledgment. We thank V. F. Puentes for many helpful conversations on the synthesis and magnetic properties of Co nanoparticles. Assistance from B. L. Kirsch and A. E. Riley with low-angle XRD scattering is appreciated. This manuscript includes data collected at the Stanford Synchrotron Radiation Laboratory (SSRL), which is operated by the Department of Energy, Office of Basic Energy Sciences. This work was supported by the Beckman Foundation, the Office of Naval Research (N00014-99-1-0568), and the Department of Energy (DE-FG03-01ER45949). S.H.T. is an Alfred P. Sloan Foundation Research Fellow.

References and Notes

- (1) Diehl, M. R.; Yu, J.-Y.; Heath, J. R.; Held, G. A.; Doyle, H.; Sun, S.; Murray, C. B. *J. Phys. Chem. B* **2001**, *105*, 7913.
- (2) Leslie-Pelecky, D. L.; Rieke, R. D. *Chem. Mater.* **1996**, *8*, 1770.
- (3) Néel, L. C. *R. Acad. Sci.* **1949**, 228, 664.
- (4) Sun, S.; Murray, C. B.; Weller, D.; Folks, L.; Moser, A. *Science* **2000**, *287*, 1989.
- (5) Sun, S.; Fullerton, E. E.; Weller, D.; Murray, C. B. *IEEE Trans. Magn.* **2001**, *37*, 1239.
- (6) Thurn-Albrecht, T.; Schotter, J.; Kästle, G. A.; Emley, N.; Shibauchi, T.; Krusin-Elbaum, L.; Guarini, K.; Black, C. T.; Tuominen, M. T.; Russell, T. P. *Science* **2000**, *290*, 2126.
- (7) Jacobs, I. S.; Bean, C. P. *Phys. Rev.* **1955**, *100*, 1060.
- (8) Sun, S.; Murray, C. B. *J. Appl. Phys.* **1999**, *85*, 4325.
- (9) Dinega, D. P.; Bawendi, M. G. *Angew. Chem., Int. Ed. Engl.* **1999**, *38*, 1788.
- (10) Puentes, V. F.; Krishnan, K. M.; Alivisatos, A. P. *Science* **2001**, *291*, 2115.
- (11) Puentes, V. F.; Zanchet, D.; Erdonmez, C. K.; Alivisatos, A. P. *J. Am. Chem. Soc.* **2002**, *124*, 12874.
- (12) Legrand, J.; Petit, C.; Pileni, M. P. *J. Phys. Chem. B* **2001**, *105*, 5643.
- (13) Sun, S.; Zeng, H. *J. Am. Chem. Soc.* **2002**, *124*, 8204.
- (14) Fried, T.; Shemer, G.; Markovich, G. *Adv. Mater.* **2001**, *13*, 1158.
- (15) Shevchenko, E. V.; Talapin, D. V.; Rogach, A. L.; Kornowski, A.; Haase, M.; Weller, H. *J. Am. Chem. Soc.* **2002**, *124*, 11480.
- (16) Kurikka, V.; Shafi, P. M.; Felner, I.; Mastai, Y.; Gedanken, A. *J. Phys. Chem. B* **1999**, *103*, 3358.
- (17) Son, S.; Taheri, M.; Carpenter, E.; Harris, V. G.; McHenry, M. E. *J. Appl. Phys.* **2002**, *91*, 7589.
- (18) Khan, M. L.; Zhang, Z. *J. Appl. Phys. Lett.* **2001**, *78*, 3651.
- (19) Grasset, F.; Labhsetwar, N.; Li, D.; Park, D. C.; Saito, N.; Haneda, H.; Cadot, O.; Roisnel, T.; Mornet, S.; Duguet, E.; Portier, J.; Etourneau, J. *Langmuir* **2002**, *18*, 8209.
- (20) Murray, C. B.; Sun, S.; Gaschler, W.; Doyle, H.; Betley, T. A.; Kagan, C. R. *IBM J. Res. Dev.* **2001**, *45*, 47.
- (21) Held, G. A.; Grinstein, G.; Doyle, H.; Sun, S.; Murray, C. B. *Phys. Rev. B* **2001**, *64*, 2408.
- (22) Zhao, D.; Feng, J.; Huo, Q.; Melosh, N.; Fredrickson, G. H.; Chmelka, B. F.; Stucky, G. D. *Science* **1998**, *279*, 548. Zhao, D.; Huo, Q.; Feng, J.; Chmelka, B. F.; Stucky, G. D. *J. Am. Chem. Soc.* **1998**, *120*, 6024.
- (23) Zhang, L.; Manthiram, A. *Phys. Rev. B* **1996**, *54*, 3462.
- (24) Bottoni, G.; Candolfo, D.; Cecchetti, A.; Masoli, F. *J. Magn. Magn. Mater.* **1992**, *116*, 285.
- (25) Franco, V.; Batlle, X.; Labarta, A.; O'Grady, K. *J. Phys. D: Appl. Phys.* **2000**, *33*, 609.
- (26) Zeng, H.; Sun, S.; Vedantam, T. S.; Liu, J. P.; Dai, Z.-R.; Wang, Z.-L. *J. Appl. Phys. Lett.* **2002**, *80*, 2583.
- (27) Zeng, H.; Li, J.; Liu, J. P.; Wang, Z. L.; Sun, S. *Nature* **2002**, *420*, 395.
- (28) Kresge, C. T.; Leonowicz, M. E.; Roth, W. J.; Vartuli, J. C.; Beck, J. S. *Nature* **1992**, *359*, 710. Beck, J. S.; Vartuli, J. C.; Roth, W. J.; Leonowicz, M. E.; Kresge, C. T.; Schmitt, K. T.; Chu, C. T.-W.; Olson, D. H.; Sheppard, E. W.; McCullen, S. B.; Higgins, J. B.; Schlenker, J. L. *J. Am. Chem. Soc.* **1992**, *114*, 10834.
- (29) Gross, A. F.; Le, V. H.; Kirsch, B. L.; Riley, A. E.; Tolbert, S. H. *Chem. Mater.* **2001**, *13*, 3571.
- (30) Huo, Q.; Margolese, D. I.; Stucky, G. D. *Chem. Mater.* **1996**, *8*, 1147.
- (31) Gallis, K. W.; Landry, C. C. *Chem. Mater.* **1997**, *9*, 2035.
- (32) Zhao, D.; Huo, Q.; Feng, J.; Kim, J.; Han, Y.; Stucky, G. D. *Chem. Mater.* **1999**, *11*, 2668.
- (33) Gross, A. F.; Le, V. H.; Kirsch, B. L.; Tolbert, S. H. *Langmuir* **2001**, *17*, 3496.
- (34) Han, Y.-J.; Kim, J. M.; Stucky, G. D. *Chem. Mater.* **2000**, *12*, 2068.
- (35) Gao, F.; Lu, Q.; Yan, Y.; Zhao, D. *Nano Lett.* **2001**, *1*, 743.
- (36) Fukuoka, A.; Araki, H.; Sakamoto, Y.; Sugimoto, N.; Tsukada, H.; Kumai, Y.; Akimoto, Y.; Ichikawa, M. *Nano Lett.* **2002**, *2*, 793.
- (37) Shin, H. J.; Ryoo, R.; Liu, Z.; Terasaki, O. *J. Am. Chem. Soc.* **2001**, *123*, 1246.
- (38) Konya, Z.; Puentes, V. F.; Kiricsi, I.; Zhu, J.; Alivisatos, A. P.; Somorjai, G. A. *Nano Lett.* **2002**, *2*, 907.
- (39) Wu, J. J.; Gross, A. F.; Tolbert, S. H. *J. Phys. Chem. B* **1999**, *103*, 2374; Nguyen, T. Q.; Wu, J. J.; Doan, V.; Schwartz, B. J.; Tolbert, S. H. *Science* **2000**, *288*, 652.
- (40) Murray, S.; Trudeau, M.; Antonelli, D. M. *Inorg. Chem.* **2000**, *39*, 5901.
- (41) Jirage, K. B.; Hulteen, J. C.; Martin, C. R. *Science* **1997**, *278*, 655.
- (42) Routkevitch, D.; Bigioni, T.; Moskovits, M.; Xu, J. M. *J. Phys. Chem.* **1996**, *100*, 14037.
- (43) Wong, J.; Scherer, A.; Barbic, M.; Schultz, S. *J. Vac. Sci. Technol. B* **1999**, *17*, 3190.
- (44) Guinier, A. *X-ray Diffraction in Crystals, Imperfect Crystals, and Amorphous Bodies*; Dover: New York, 1994.
- (45) Stoner, E. C.; Wohlfarth, E. P. *Philos. Trans. R. Soc. London, Ser. A* **1948**, *240*, 599.
- (46) Ohshima, K. *J. Magn. Magn. Mater.* **1989**, *79*, 276.
- (47) Cowburn, R. P. *Phys. Rev. B* **2002**, *65*, 092409.